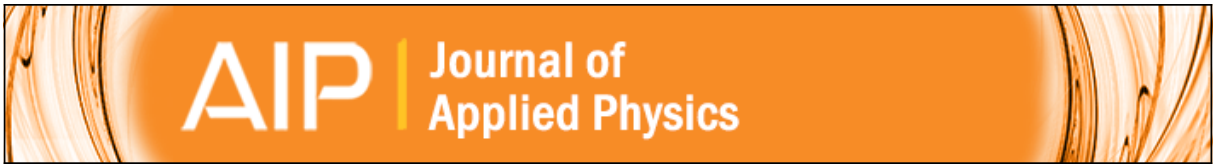

Deterministic control of plasma-assembled self-organized Ge Si quantum dot arrays

J. C. Ho, I Levchenko, and K. Ostrikov

Citation: Journal of Applied Physics **101**, 094309 (2007); doi: 10.1063/1.2727448

View online: http://dx.doi.org/10.1063/1.2727448

View Table of Contents: http://scitation.aip.org/content/aip/journal/jap/101/9?ver=pdfcov

Published by the AIP Publishing

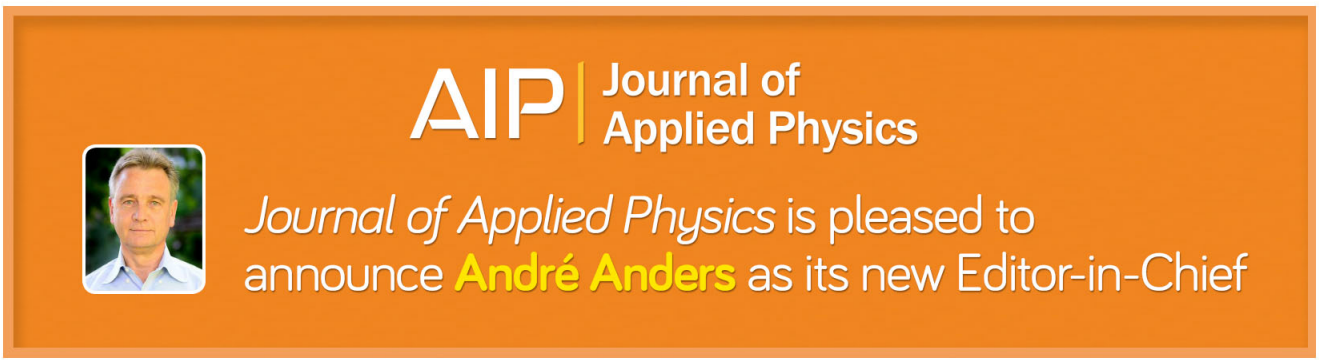

Deterministic control of plasma-assembled self-organized Ge/Si quantum dot arrays

J. C. Ho, I Levchenko, and K. Ostrikov[a)]
Plasma Nanoscience@Complex Systems, School of Physics, The University of Sydney, Sydney NSW 2006, Australia

(Received 20 February 2007; accepted 6 March 2007; published online 11 May 2007)

Self-assembly of size-uniform and spatially ordered quantum dot (QD) arrays is one of the major challenges in the development of the new generation of semiconducting nanoelectronic and photonic devices. Assembly of Ge QD (in the $\sim 5-20$ nm size range) arrays from randomly generated position and size-nonuniform nanodot patterns on plasma-exposed Si(100) surfaces is studied using hybrid multiscale numerical simulations. It is shown, by properly manipulating the incoming ion/neutral flux from the plasma and the surface temperature, the uniformity of the nanodot size within the array can be improved by 34%–53%, with the best improvement achieved at low surface temperatures and high external incoming fluxes, which are intrinsic to plasma-aided processes. Using a plasma-based process also leads to an improvement ($\sim$22% at 700 K surface temperature and 0.1 ML/s incoming flux from the plasma) of the spatial order of a randomly sampled nanodot ensemble, which self-organizes to position the dots equidistantly to their neighbors within the array. Remarkable improvements in QD ordering and size uniformity can be achieved at high growth rates (a few nm/s) and a surface temperature as low as 600 K, which broadens the range of suitable substrates to temperature-sensitive ultrathin nanofilms and polymers. The results of this study are generic, can also be applied to nonplasma-based techniques, and as such contributes to the development of deterministic strategies of nanoassembly of self-ordered arrays of size-uniform QDs, in the size range where nanodot ordering cannot be achieved by presently available pattern delineation techniques. © *2007 American Institute of Physics*.
[DOI: 10.1063/1.2727448]

I. INTRODUCTION

Zero-dimensional semiconductor quantum dot (QD) structures have recently been the subject of intense research efforts due to unique size-dependent electronic properties resulting from electron confinement in all three dimensions.[1,2] The intrinsic ability of QDs to emit light and generate single-electron currents makes them particularly attractive for various advanced applications spanning a broad range of fields from bionanotechnology to nano-photonics, optoelectronics, and quantum computing.[3–6] Examples of the most commmon semiconducting nanodot systems include, but are not limited to, Ge, Si, GaAs, InSb, InAs, and AlN on a range of host materials such as Si, SiO_2, AlN, etc.

One of the main issues in the development of QD-based nanodevices is the ability to arrange QDs with the same size, shape, structure, etc. in regular, uniform spatial arrays. Such an arrangement greatly enhances the collective optoelectronic properties of the QDs through coupling interactions within the ensemble. In particular, these interactions substantially improve the efficiency and intensity of photoemissions in numerous applications including QD laser and biomedical tagging devices.[7–11] Moreover, ultrafine tuning of the emission frequency can be achieved by controlling the size and positioning of QDs within an array. Therefore, nanodevice applications utilizing of QD systems will ultimately require a high level of QD size uniformity and positional ordering.[12]

Many existing pattern delineation techniques provide a reasonable level of control over QD position yet cannot meet the requirements for the size and shape uniformity of individual QDs.[13] Hybrid techniques involving lithographic prepatterning and follow-up site-controlled self-organized growth of QDs have also been attempted.[9,14] However, due to intrinsic resolution-related limitations, prepatterning techniques are not suitable for nanofabrication of ordered QD arrays compatible with the emerging sub-40 nm semiconductor technology, which will essentially rely on *bottom-up* self-assembly approaches.[15] Moreover, QDs with the sizes larger than 40 nm are not practical to meet the continuously rising demands for the surface coverage and nanodot density. A further limit to top-down approaches is the difficulty in achieving uniform distributions in QD sizes and shapes.

Therefore, controlled self-organization is the most promising way to overcome the above difficulties and deterministically fabricate nanodot arrays with attributes suitable for their eventual nanodevice applications. The effectiveness of this approach critically depends on the nanofabrication environment used and the ability to create and manipulate nanoassembly building units.[16]

Plasma-based environments have recently exhibited superior performance in the synthesis of various nanostructures and nanoassemblies including nanotubes, nanowires, and QD arrays (QDAs) made of a variety of materials and suitable for

[a)]Author to whom correspondence should be addressed. Electronic mail: k.ostrikov@physics.usyd.edu.au

numerous advanced applications.[16–24] Here, by means of multiscale hybrid numerical simulations we demonstrate that plasma-assisted nanofabrication can be used to achieve deterministic control of the positional order and size uniformity of Ge/Si QDs. This is one of the most commonly used semiconducting systems possessing unique optoelectronic properties, a lattice mismatch of ~4% and widespread industrial applications.[25–27]

Self-organized growth of Ge/Si QDs usually proceeds via strain-induced fragmentation of a continuous Ge film into nanoislands, commonly referred to as the Stranski-Krashtanov growth mode.[28] As a result, nonuniform patterns of size-nonuniform nanoislands are formed. Here we attempt to show that these irregular nanoisland patterns can be improved using a plasma-based process and can eventually be brought to the level required for nanodevice applications.

More specifically, we report on a generic and versatile plasma-based approach that makes it possible to substantially improve the size uniformity of individual Ge QDs and their positional uniformity in originally nonuniform nanopatterns on plasma-exposed Si(100) surfaces. The approach is based on the precise manipulation of both the incoming fluxes of plasma-generated building units (BUs) and the surface temperature. This leads to a rearrangement of the two-dimensional (2D) surface adatom fluxes, which in turn results in faster growth of smaller dots and eventually better QD size uniformity. On the other hand, quasi-displacement of QDs due to unbalanced surface adatom fluxes from different directions results in a more equidistant positioning of the dots with respect to their neighbors within the array.

This paper has the following structure. In the following section (Sec. II) we introduce the numerical model of the growth and movement of QDs subjected to particle fluxes from the plasma and adatom diffusion over the substrate surface. In Sec. III the results of the numerical study of the effect of variation of the process parameters on the size uniformity and positional order of the Ge nanodots are presented. Section IV explains the results of the numerical simulations and comments on practical deterministic control strategies for plasma-aided nanoassembly of ordered and size-uniform Ge/Si QD arrays. The paper concludes with a summary of the main results and directions for future research.

II. FORMULATION

Here, a numerical technique, which combines aspects of the delivery of building units from the plasma bulk with the diffusion of adatoms on a Si substrate is used to model QD growth and displacement on a plasma-exposed Si(100)surface. The non-neutral layer between these two regions, the plasma sheath, plays an important role in the nondestructive delivery of building units transported from the plasma toward the solid surface. The potential distribution across the sheath results in the intense ion fluxes allowing one to maintain even and constant substrate temperatures. Moreover, the ion flux control can be achieved through the variation of the substrate bias potential. On the other hand, the operating pressure turns out to be the main control of the neutral fluxes from the plasma discharge.

Here we investigate the growth and displacement of Ge/Si QDs arranged in a nonuniform nanopattern subjected to incoming fluxes of germanium atoms and ions from the plasma environment. In simulations, we used a rectangular $1\ \mu m \times 1\ \mu m$ nanopattern with 400 dome-shaped nanodots arranged randomly to reproduce typical distributions of Ge nanoislands on a silicon surface.[29–32] The initial QD sizes range from 4 to 13 nm and are assumed to possess a Gaussian distribution. We emphasize that our model is generic and applicable to a broad range of plasma nanotools; thus, we do not specify the exact way the plasma is generated and the range of species that it can produce. Furthermore, it is assumed that only germanium adatoms act as building units of Ge QDs on a Si surface. Although other neutral or ionized species in the plasma may facilitate this process, they are not explicitly accounted for in the model. For example, a controlled flux of Ge^+ ions can be achieved via the argon plasma-facilitated ionized physical vapor deposition (IPVD); in this case the argon plasma serves the purpose of ionizing Ge atoms and also activating silicon surface.[16,33] Upon deposition onto a silicon surface, Ge ions are neutralized and become adatoms, the main contributors to the Ge/Si QD growth. We used the values of the incoming fluxes of Ge^+ ions and Ge atoms consistent with relevant experiments on synthesis of Ge/Si and related QD systems in low-pressure plasmas.[22–24] The pressure range considered was 5–100 mTorr. The ionization degree was varied from $\sim 10^{-3}$ representative of high-density, low-pressure rf plasmas commonly used for microelectronic fabrication to ~0.5, which is typical for advanced pulsed IPVD systems.

In the model adopted here, the primary variable simulation parameters are the Si substrate surface temperature and the incoming external flux of Ge BUs from the plasma. Our numerical experiments suggest that an optimum combination of these parameters can lead to a high level of deterministic control over the spatial or dimensional order of the Ge/Si QDs we are interested in. Furthermore, we comment on the effectiveness of each control parameter in every case; this can facilitate the practical implementation of our results.

Figure 1(a) shows a schematic of the process of Ge/Si QD deposition in a plasma-based process. In this process, germanium atoms are delivered from the ionized gas environment either directly to the nanodot or via the wafer surface. Upon contact with the Si(100) substrate, Ge adatoms migrate about the surface via surface diffusion. Depending on the surface temperature, adatoms may re-evaporate from the QD either to the 2D adatom field or back into the plasma bulk.

The hybrid QD growth model implemented in this paper is based on a set of adatom flux balance equations, which takes into consideration incoming fluxes from the plasma, fluxes due to surface diffusion and a range of adatom evaporation processes. This method has been commonly employed in surface science as a means for modeling a broad range of growth processes.[34] An additional scale has been included in this study to better describe the quasi-displacement of a large

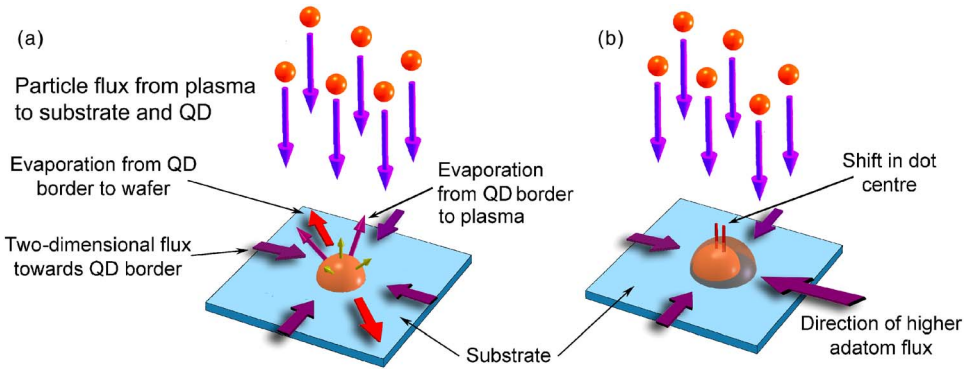

FIG. 1. (Color online) Schematics of (a) QD growth in a uniform adatom field and (b) quasi-displacement of QD center in nonuniform adatom field.

number of individual QDs. Thus, our model can be considered as a hybrid multiscale model. Previous efforts[35,36] at modeling QD nanoassembly have been attempted, however, this model is generic in that it does not specify the way of preparation of the initial patterns of seed nuclei.

In our model, the growth process of the ith QD is described by[37,38]

$$(\partial V_i/\partial r_i)dr_i = \lambda_{\text{lat}}^3 \Psi_i dt, \tag{1}$$

where λ_{lat} is the lattice constant, V_i and r_i are the ith nanodot's volume and radius, respectively, and t is the time into the growth process. Here

$$\Psi_i = \Psi_{\text{pl},i} + \Psi_{\text{surf},i} - \Psi_{\text{vap},i} - \Psi_{\text{svap},i} \tag{2}$$

is the total flux of species to the ith QD, where $\Psi_{\text{pl},i}$ is the incoming BU flux from the plasma, $\Psi_{\text{surf},i}$ is the 2D surface flux of adatoms onto the border of the ith nanodot, and $\Psi_{\text{vap},i}$ and $\Psi_{\text{svap},i}$ are the bulk and surface evaporation fluxes from the ith QD, respectively.

The incoming flux from the plasma

$$\Psi_{\text{pl},i} = \Psi_{\text{pl},i}^{\text{ion}} + \Psi_{\text{pl},i}^{n} \tag{3}$$

involves contributions from the ion and neutral fluxes represented by the first and the second terms in this equation, respectively. Here, $\Psi_{\text{pl},i}^{\text{ion}} = \int_{S_i} j_S ds_i$ and $\Psi_{\text{pl},i}^{n} = \bar{S}\psi_n$ where j_{S_i} is the density of the ion flux onto the nanodot surface with the area S_i, and ψ_n is the density of the neutral flux; the latter is assumed to be uniform over the entire substrate surface.

The 2D surface flux of adatoms is

$$\Psi_{\text{surf},i} = -D_S l_i [\nabla \eta(x,y,t)]_{l_i} \tag{4}$$

where $[\nabla \eta(x,y,t)]_{l_i}$ denotes the gradient of the adatom surface density $\eta(x,y,t)$ at the border of the ith QD with the perimeter l_i, and

$$D_S = [\nu_a \lambda_{\text{lat}}^2/4]\exp(-\varepsilon_d/k_B T_s),$$

is the surface diffusion coefficient. Here, ν_a is the characteristic frequency of atom oscillations in a lattice, ε_d is the surface diffusion activation energy, T_s is the temperature of the silicon surface, and k_B is the Boltzmann's constant.

The time-varying density of Ge adatoms on the Si(100) surface has been numerically obtained from the two-dimensional diffusion equation

$$\frac{\partial \eta(x,y,t)}{\partial t} = D_S \nabla_{2D}^2 [\eta(x,y,t)] + \psi_{\text{in}} - \psi_{\text{evap}}, \tag{5}$$

where $\nabla_{2D}^2 = \partial^2/\partial x^2 + \partial^2/\partial y^2$, and $\psi_{\text{in}} = \psi_{\text{in}}^{\text{ion}} + \psi_n$ is the incoming flux of the ionic (first term) and neutral (second term) BUs from the plasma onto open surface areas uncovered by the QDs. Here, $\psi_{\text{in}}^{\text{ion}} = [1/\bar{S}]\int_{\bar{S}} j_S d\bar{s}$, where j_S is the density of the ion flux onto the substrate surface between the QDs (area $\bar{S}$). In the rhs of Eq. (5),

$$\psi_{\text{evap}} = [\nu_a/\lambda_{\text{lat}}^2]\exp(-\varepsilon_{\text{evap}}^S/k_B T_s)$$

is the flux of adatom evaporation (with the characteristic energy $\varepsilon_{\text{evap}}^S$) from the substrate surface between the QDs.

The remaining two terms in Eq. (2), $\Psi_{\text{vap},i}$ and $\Psi_{\text{svap},i}$ represent evaporative losses from the ith QD to the gas phase and the 2D surface gas vapor, respectively. More specifically

$$\Psi_{\text{vap},i} = [\nu_a S_i/\lambda_{\text{lat}}^2]\exp(-\varepsilon_{\text{evap}}^{3D}/k_B T_s)$$

and

$$\Psi_{\text{svap},i} = [\nu_a l_i/\lambda_{\text{lat}}]\exp(-\varepsilon_{\text{evap}}^{2D}/k_B T_s),$$

where $\varepsilon_{\text{evap}}^{3D}$ and $\varepsilon_{\text{evap}}^{2D}$ are the energies of adatom evaporation to the three-dimensional (3D) vapor in the plasma bulk and the 2D vapor on the surface, respectively.

The QD growth is determined by the 2D field of microscopic adatom diffusion across its circular border. If adatom fluxes from different directions are balanced, the dots grow at the same position [Fig. 1(a)], otherwise we observe nanodot quasi-displacement sketched in Fig. 1(b). To quantify this displacement, we have decomposed the surface flux term

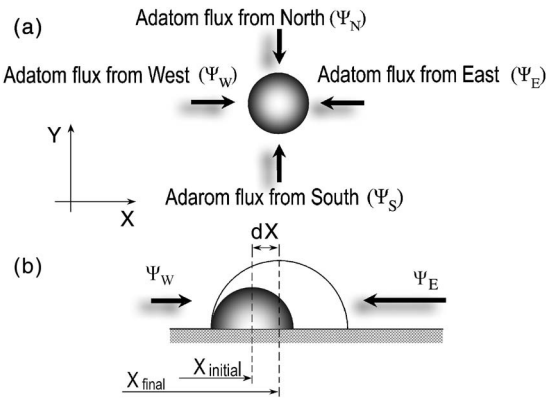

FIG. 2. Schematic of (a) the 2D flux on a QD and (b) the QD center shift through a nonuniform 2D adatom flux.

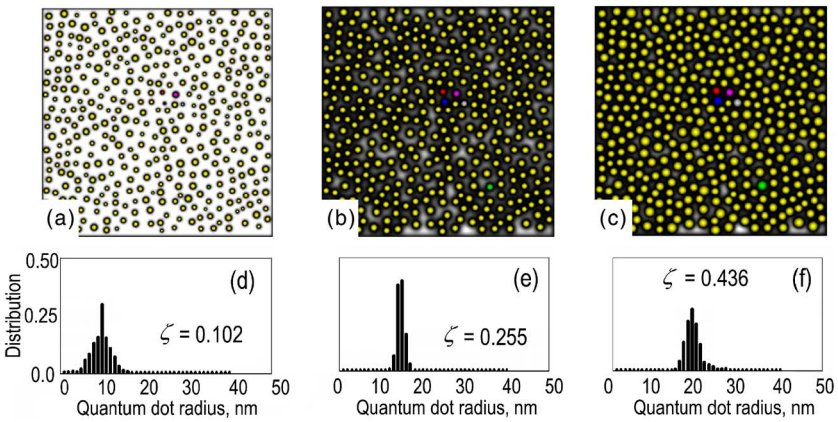

FIG. 3. QD pattern (a)–(c) and QD size distribution (d)–(f) for a surface temperature of 600 K and flux Ψ_{pl} =0.1 ML/s ($\Psi_{pl}^{ion}=0.3\Psi_{pl}$) for surface coverage (left to right) of 0.102 (a) and (d); 0.255 (b) and (e); and 0.436 (c) and (f).

entering Eq. (2) into four components Ψ_N, Ψ_S, Ψ_E, and Ψ_W directed to the North, South, East, and West, respectively (Fig. 2). The quasi-displacement of the dots within the ensemble is described as their asymmetric growth and the net shift of the QD centers resulting from differential influxes in the 2D adatom field as shown in Fig. 2.

Referring to Fig. 2, one can define the 2D positional shift (dX, dY) of a nanodot center subjected to 2D surface fluxes as

$$dX = \frac{\xi_x}{\sqrt{\xi_x^2 + \xi_y^2}} \frac{dr}{2}$$

and

$$dY = \frac{\xi_y}{\sqrt{\xi_x^2 + \xi_y^2}} \frac{dr}{2},$$

where $\xi_x=(\Psi_W-\Psi_E)/(\Psi_W+\Psi_E)$ and $\xi_y=(\Psi_N-\Psi_S)/(\Psi_N+\Psi_S)$ are the flux differential terms, and we recall that r is the (time-varying) QD radius; subscript i has been omitted for simplicity.

III. RESULTS

In this section, the results obtained via the numerical simulation of germanium QD growth and displacement on a Si(100) surface are presented. We consider the dynamics of the QD self-organization in a randomly generated starting pattern. First, the effect of the surface temperature and incoming flux on nanodot size uniformity is studied; and second, the dynamics of QD displacement will be presented demonstrating the possibility of their positional self-ordering.

A. Size uniformity

The results in Figs. 3 and 4 show the simulated QD nanopatterns at different incoming fluxes and two surface temperatures of 600 and 900 K, respectively. Comparing Figs. 3 and 4 it is seen that changed simulation parameters produce different levels of size uniformity as indicated by the broader size distributions in Fig. 4. The temporal dynamics of the dot growth displayed in Fig. 3 shows an initial wide distribution in the size of QDs, which narrows at surface coverage ζ=0.255 and then broadens again at ζ=0.436. This narrowing evidences the improvement from the initial pattern with surface coverage ζ=0.102 and subsequent deterioration in the size uniformity. The effect of the surface temperature and the plasma influx on standard deviation in QD size shown in Fig. 5 gives further evidence to this effect. Thus, the uniformity in the nanodot size initially improves from the starting seed nuclei pattern but is followed by a steady deterioration in uniformity when a certain surface coverage is achieved.

The results in Fig. 5(a) indicate that QD mean radius and the level of size uniformity are dependent on the surface temperature of the Si wafer. It appears that with increasing T_s there is a decrease in the mean dot radius at the points of the optimum size uniformity (flex points in Fig. 5). It is also seen that the improvement (as compared to the initial pattern) in

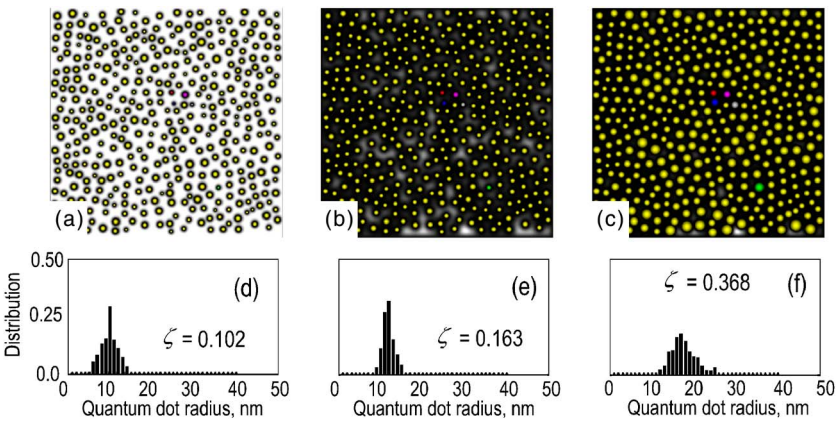

FIG. 4. Same as in Fig. 3 for T_s =900 K and surface coverage (left to right) of 0.102 (a) and (d); 0.163 (b) and (e); and 0.368 (c) and (f).

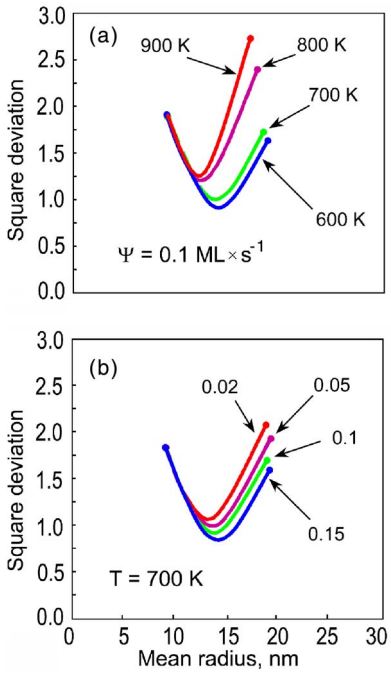

FIG. 5. (Color online) Standard deviation in QD size within the ensemble for different (a) surface temperatures at Ψ_{pl}=0.1 ML/s and (b) incoming fluxes at T_s=700 K. The ion flux is the same as in Fig. 3.

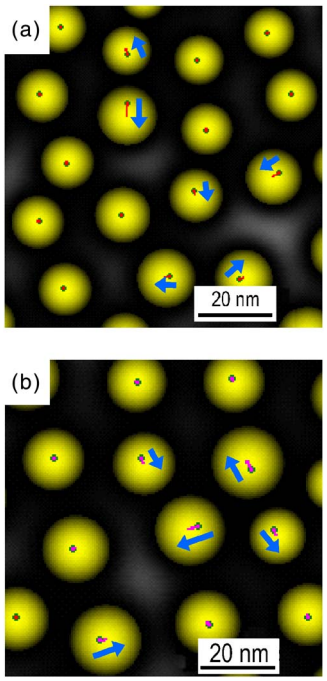

FIG. 6. (Color online) Enlarged QD patterns at two different sites on a wafer with marked centers showing displacements toward the areas of lower surface coverage.

the QD size uniformity is not as marked for higher surface temperatures; in this case the turn-off point appears at smaller mean nanodot radii (and hence at lower surface coverages) as can be seen from Fig. 5(a).

Figure 5(b) shows the square deviation of the QD sizes from the mean nanodot size in the nanopattern for different incoming fluxes. The results of our numerical experiments suggest that higher Ψ_{pl} merely lead to a modest increase of the mean QD size. As an example, for incoming flux between 0.02 and 0.15 ML/s, the change in the mean QD radius when the size uniformity is the best [minima in Fig. 5(b)] does not exceed ~2 nm. It is also seen that the optimum achievable uniformity is obtained using higher incoming fluxes. Indeed, the smallest possible square deviation of the nanodot sizes (~0.8) can be obtained when the incoming flux is set to 0.15 ML/s [Fig. 5(b)].

Therefore, the results of this subsection clearly illustrate the self-organization of the QD array to achieve a uniform QD size distribution. In fact, the results of our numerical simulations reveal that smaller dots exhibit accelerated growth while the growth of larger dots is retarded. For more discussion of this effect, see Sec. IV.

B. Positional uniformity

We now consider the results related to the positional order of QDs within the array and the dynamics of nanodot movement to achieve such an order. Figure 6 shows two randomly selected areas within the array. Directions and relative magnitudes of displacements of QD centers routinely traced in the simulations are shown by the arrows of different lengths. At these and many other sites within the array it has been repeatedly observed that the dot movement followed predictable routes from highly occupied (by neighboring QDs) toward less occupied regions of the wafer. In the top right section of Fig. 6(a) it is seen that two dots in close proximity appear to move in opposite directions while at the center of Fig. 6(b) the nanodot is observed to move into a vacant space.

To elucidate the motion dynamics of five selected QDs (labeled 1–5), in Fig. 7, plots of dot-specific radii, displacements from initial positions, and velocities associated with the quasi-displacements are presented alongside with the three snapshots of the same nanopattern with these dots at three different time moments. Figure 7 corresponds to a typical surface temperature of 700 K with a 0.1 ML/s incoming flux. In particular, Fig. 7(f) indicates that smaller QDs appear to move faster. In fact, upon closer evaluation of Figs. 7(e) and 7(f), the QD labeled (1) moves with a considerably lower velocity (and is displaced by a smaller distance) than its more mobile counterparts (2) and (3) despite their similar size evidenced by Fig. 7(d). Physically, this is caused by the difference in the relative location of the dots with respect to their neighbors. Examining the QD patterns in Fig. 7 it is seen that the QD labeled (1) is positioned centrally such that its distance to the adjacent neighbors is approximately the same. On the contrary, the dots labeled (2) and (3) are positioned asymmetrically with respect to their neighbors.

From Fig. 8 one can notice that a local site with a QD in the middle self-organizes to equalize the distances between the central dot and its neighbors. In this example, Fig. 8(a) shows that the central dot is initially positioned closer to its neighbors on the left. After only 0.14 s into the deposition process at T_s=700 K and Ψ_{pl}=0.1 ML/s the same dot has equally positioned itself between its right- and left-side neighbors following quite minor quasi-displacements of all the nanodots in the ensemble, as evidenced by Fig. 8(b). In

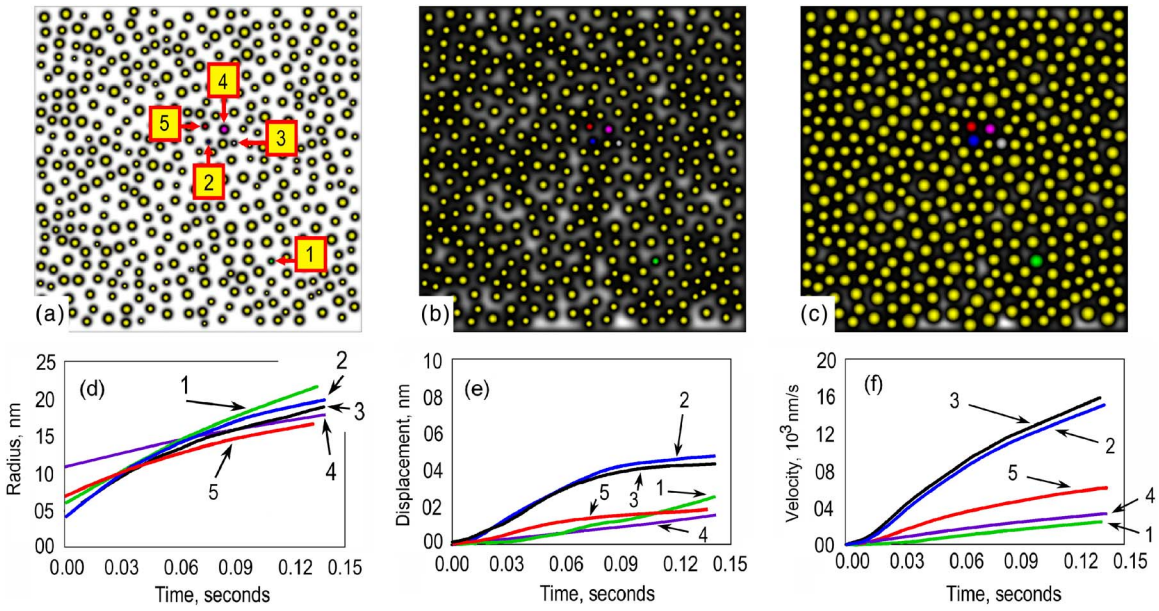

FIG. 7. (Color online) QD pattern and adatom field at (a) 0, (b) 0.035, and (c) 0.141 s. Temporal evolution of (a) radii, (b) displacement, and (c) velocity values for selected QDs of the initial size: (1) 6 nm (green); (2) 4 nm (blue); (3) 5 nm (gray); (4) 11 nm (magenta); and (5) 7 nm (red).

fact, the ratio of the most-unequal distances (labeled in the figure) changed from 0.7 for the initial state to 0.96 for the final pattern.

Thus, numerical experiments suggest that the growth of individual QDs is affected by their relative size and vicinity to neighboring dots. In fact, smaller dots located in an area of a low local surface coverage usually experience an accelerated growth as compared to larger QDs located in close proximity to nearby nanodots.

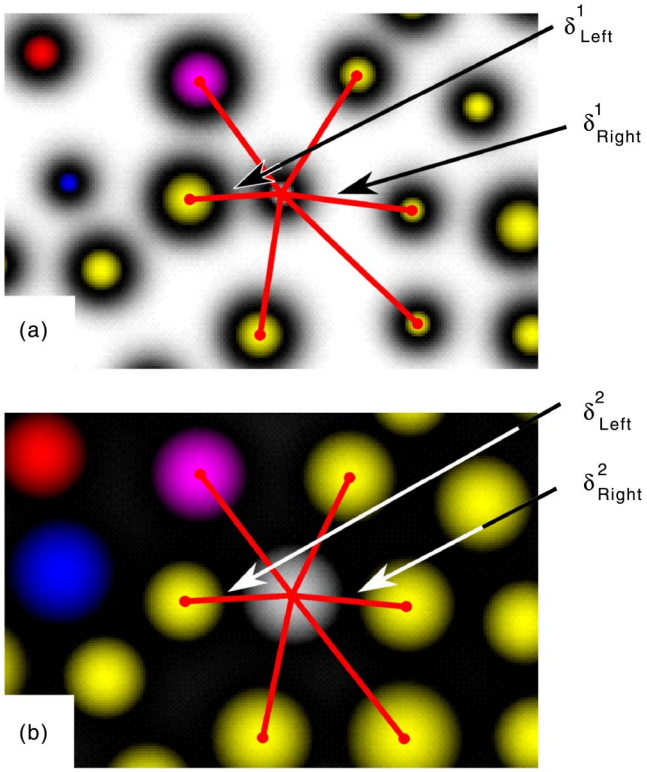

FIG. 8. (Color online) QD pattern at (a) start (t=0 s) and (b) end (t=0.14 s) of the growth simulation showing the distance of a dot (gray) to its neighbors for surface temperature 700 K and external flux 0.1 ML/s. The ion flux is the same as in Fig. 3. The distances seem to become more uniform.

IV. DISCUSSION

Before we proceed further, it should be stressed that despite a large number of reports on self-organization phenomena in complex physical systems, it is still unclear as to what is the common driving force of such an amazing phenomena. It is understood, however, that the physical mechanisms responsible for the self-organization are numerous and case-specific. The key to self-organization in the plasma-surface environment of our interest is the collective behavior of neutral and ionized building units, BU transport via the plasma sheath followed by their surface migration, collisions, clustering, and self-assembly into specific nanostructures on the solid surface.[16]

If properly understood and controlled through manipulation of the plasma and surface parameters and initial conditions, this self-organization phenomenon may be harnessed to enable deterministic nanofabrication of nanodevice-grade QD arrays. This paper has attempted to elucidate some plausible ways to create ordered Ge/Si QDAs in a plasma-assisted process by manipulating the incoming fluxes from the plasma and the surface temperature.

The results of our numerical experiments suggest that QDs grow faster in the areas with a lower local surface coverage. Moreover, QDs displace themselves in appearing to establish uniform size and distance in relation to their neighbors. Individual QDs appear to move into spaces with the lower surface coverage ζ but higher adatom number density. We should mention here that the QD itself does not actually move on the substrate surface (we examine the QDs of 10–20 nm which cannot move about the surface such as adatoms), and thus we consider actually the displacement of the QDs centers due to the non-symmetric QDs growth. The

apparent cause for this displacement is the unbalanced 2D adatom fluxes (Fig. 2). Examining Fig. 3 one can see that the adatom density shown as a gray field in Figs. 3(a)–3(c) is higher in surface zones between the distant QDs. As a result, the increased adatom fluxes from the surface zones of higher density cause an increased irregular growth of the QDs and finally displacement of their centers, usually toward higher adatom densities. Finally, the QDs arrange themselves within the 2D adatom field in order to maintain or achieve uniform adatom fluxes about their perimeter.

This behavior presents an undeniable picture of the self-organization phenomena in this plasma system. Once the mechanisms behind this self-organization are established, the next stage is to harness them in practical applications that require self-assembled, highly ordered arrays of size-uniform QDs. It is worth noting that the results of our numerical simulations appear to qualitatively resemble those Ge/Si(100) QD patterns synthesized experimentally.[32,39] In the situations considered in this study, the growth and movement of QDs have been clearly influenced by the 2D nonuniform field of the surface adatom fluxes. Therefore, one can state that the plasma-aided approach considered here is an effective self-organization route wherein BUs from the plasma are deposited onto a solid surface and then contribute to self-assembly of ordered arrays of size-uniform QDs. We emphasize that the self-assembly of individual QDs and their self-ordering into self-organized nanoarrays makes it possible to fabricate such nanoassemblies without the need of a continuous external control, which is a common feature of most of self-organized complex systems.

However, as the results of our numerical experiments suggest, the plasma-based QD growth process is very fast and requires only a fraction of a second to substantially increase the nanodot size as can be seen in Figs. 3, 4, and 7. Therefore, the process should be terminated at the point where the best size uniformity and/or positional ordering are achieved.

The specific conditions that enable the best nanodot uniformity can be deduced using the results displayed in Fig. 5. As seen in Fig. 5(a), an increase of the surface temperature from 600 to 900K results in a net decrease in the QD mean radii when the nanopattern uniformity is the optimum (square deviation is minimal). An important feature in Fig. 5(a) is the presence of well-resolved minima that appear to be different when T_s is varied. We recall that these minima represent the mean radius at the critical point where the size uniformity is the best. The optimum mean radius (along with all other mean radii values) increases inversely to T_s. However, the deviation in the QD size is seen to increase with the surface temperature. A possible reason is that at lower surface temperatures a slower adatom migration extends the time of nanodot growth, eventually allowing the size deviation to settle. The relationship between the surface temperature, incoming fluxes and the QD size is, therefore, useful in achieving effective control over the nanodot nucleation density and surface coverage. However, it is important to cease the growth process at the point of the minimum size deviation to take advantage of the apparent gains in the QD size uniformity.

Therefore, we have successfully demonstrated that the Ge/Si nanodot size uniformity can indeed be effectively controlled, and in most cases, improved by appropriately manipulating the incoming fluxes and the surface temperature. However, extreme caution should be taken not to overheat the surface since the mean size deviation tends to rise with T_s; deterioration of nanodot size uniformity becomes even more apparent for larger QDs. In other words, in addition to a smaller mean radius at the critical point, higher surface temperatures have the effect of increasing the deviation in the QD size distribution in the manner shown in Fig. 5(a).

Figure 5(b) shows that a decrease from 0.15 to 0.02 ML/s in the incoming flux of building units results in a slight increase in the QD size deviation, i.e., a minor loss in the QD size uniformity. The more notable effects from this parameter are the surface coverage and the time to reach the critical point and the time to the first contact between two dots. Our simulations have clearly shown that at a lower incoming flux the QDs growth time increases. However, at the lower flux (0.05 ML/s) the final coverage upon contact is greater than that at the higher flux (0.1 ML/s). It is noteworthy that at lower Ψ_{pl}, QDs are given ample time to reposition their centers into the vacant regions before they can enlarge and eventually coalesce; this can result in a substantial degeneration of order. Thus, despite the lower flux of atoms landing on the substrate, the ultimate surface coverage is increased over a longer period as the QDs are permitted to grow longer. This trend is not the case at the critical point when the QD size uniformity is the best. For the lower flux case, the coverage at this point is $\zeta=0.21$ compared to the higher-flux coverage of 0.23. This difference shows that the surface coverage is indeed larger at higher Ψ_d. Interestingly, once a sufficient amount of the adatoms is available, the nanodot quasi-displacement is initiated with the net effect of increasing the final coverage. Lower incoming fluxes from the plasma can, therefore, be used as a way of improving the surface coverage at the point of coalescence (QD contact). However, it is more useful to improve the surface coverage at the critical point when the dots are the most uniform in size; this can be achieved using higher incoming fluxes from the plasma instead.

Tables I–III quantify the improvement of the spatial order in localized regions of the wafer such as that seen in Fig. 8. The mean square deviation reflects on the level of uniformity in the distances of the selected central dot to adjacent QDs. Our numerical results show that the positional uniformity improves significantly in the areas of the initially high nonuniformity, with a quite different trend in the areas where the dot positioning was already uniform. In the latter case the improvement in the nanopattern order is minor or even negative. This is the case for one of the selected regions centered at the QD labeled (4), as clearly seen from the results in Table III. It is notable that selected regions containing numerous smaller dots exhibit a greater net gain in order. Due to the better ability of smaller QDs to move (evidenced by larger values of their quasi-displacements relative to their original size), this is likely to result in a greater improvement in the spatial order. The displacement of these dots has a better chance to reach a maximum before a coalescent con-

TABLE I. Physical constants and simulation parameters used in computations.

Physical constants	Value
Lattice atom oscillation frequency, ν_a (s^{-1})	1×10^{13}
Lattice parameter, λ_{lat} (m)	5×10^{-10}
Ge diffusion activation energy, ε_d (eV)	1.3
Energy of Ge evaporation to 2D vapor, ε_{evap}^{2D} (eV)	0.70
Energy of Ge evaporation to 3D vapor, ε_{evap}^{3D} (eV)	0.75
Energy of Ge evaporation from Si, ε_{evap}^{S} (eV)	0.65
Ge atom bonding energy, ε_b (eV)	2.6
Simulation parameters	
Total influx Ψ_{pl} (ML/s)	0.01–0.15
Influx of neutrals Ψ_{pl}^{n} (ML/s)	0.006–0.1
Ion influx Ψ_{pl}^{ion} (ML/s)	0.004–0.05
Initial number of QDs	400
Surface temperature, T_s (K)	600–900
Surface coverage, ζ	0.1–0.46
QD mean radius, φ (nm)	8–19
Process duration, t (s)	0–0.5
Pressure range (mTorr)	5–100
Ionization degree	$10^{-3}-0.5$

tact can be reached. Thus, in order to improve the spatial order during this growth process the initial nanodot pattern should contain seed nuclei with the minimum possible size.

In our numerical experiments we have initiated growth from randomly generated initial size and position-nonuniform nanopatterns and studied the processes of "self-uniformization" in QD sizes and self-ordering of nanodots within the developing array.

An interesting though nonsystematic observation from our numerical experiments is that the simulated spatial ordering of the QDs appears to be more sensitive to the starting pattern rather than the plasma process parameters. Apparently, if the initial nonuniformity exceeds a certain threshold, it is unlikely that perfect order can be achieved by any manipulation of the process parameters. Further studies aimed at quantifying this effect are on the way.

The large-scale control over the desired QD arrays is, therefore, likely to depend on the way the starting array has been formed. Therefore, in considering any future attempts

TABLE II. Mean radius and surface coverage for various simulation parameters at the time of the optimum size uniformity.

	Simulation parameters		QD array features set	
Set	T_s (K)	Ψ_{pl} (ML/s)	φ_{opt} (nm)	ζ_{opt}
1	600	0.1	14.23	0.255
2	600	0.05	14.2	0.255
3	600	0.02	13.9	0.244
4	700	0.1	13.35	0.229
5	700	0.05	13.33	0.224
6	700	0.02	12.69	0.203
7	800	0.1	12.1	0.186
8	800	0.05	12.08	0.185
9	800	0.02	11.9	0.156
10	900	0.1	11.7	0.173
11	900	0.05	12.0	0.182
12	900	0.02	11.7	0.172

TABLE III. Mean square deviation of distances of randomly selected QD to adjacent QDs for T_s=700 K at Ψ_{pl}=0.1 ML/s.

QD		Mean square deviation	
Number	Starting coordinate of central QD (pixels)	Initial	Final
1	(611, 421)	105.46	86.96
2	(481, 809)	145.86	103.94
3	(903, 553)	133.87	64.00
4	(215, 413)	35.16	35.75
5	(165, 215)	75.71	60.69

to create ordered arrays maximizing the spatial coherence during the early fabrication stage is strongly recommended. The extent of this preorder may allow for some divergence since according to our results, the plasma-aided QD growth makes it possible to notably improve the size uniformity of individual nanodots and the spatial order within the nanodot arrays. It is worth noting that the QD size uniformity is less sensitive to variance in the starting radius distribution, but is strongly affected by the growth parameters such as those shown in Table I. It is, therefore, possible to allow for some deviation in size when generating starting patterns. These imperfections of the initial nanopatterns should be reasonably small to be brought (during the plasma-based post-processing stage of our interest) within the acceptable tolerance of nanodevices to nonuniformities in the nanodot size and order.

We will now discuss the validity of some of the assumptions of our numerical model. In this numerical simulation we have assumed a defect-free surface and did not consider any lattice mismatch in the Ge/Si system. In reality, as was mentioned in Sec. I, the Ge/Si system features a lattice mismatch that amounts to ~4%.[40] Nevertheless, this effect is mitigated in the low coverage regime; however, as the coverage approaches the order of what is observed in this simulation ($\zeta\approx0.4$) the lattice mismatch may have some effect on the spatial order of the QDA. It must be noted, however, that in real fabrication methods involving strain-induced site-allocated growth, lattice mismatch-related effects become important at higher surface coverages than those in this study.[41] Even though our simulations have assumed a zero-defect, nonpatterned surfaces, there is no limitation in applying this plasma-aided nanoassembly model in conjunction with strain-induced growth and lithographic prepatterning methods since here we have bypassed the initial nucleation stage, which may or may not involve the SK growth scenario. For this reason, the plasma-based process of our interest here can now be seen as a powerful post-improvement tool of initially nonuniform prefabricated QD patterns.

For simplicity, the numerical model employed in this paper has assumed dome-shaped nanocrystals without considering their internal chemical structure, which in reality can undergo significant changes during the growth process. One should note that two typical dot shapes, pyramidal, and multifaceted dome shapes are most common to Ge/Si QDs.[7,42–45] Moreover, depending on the nanodot size, their real shape can change during the growth process, with dome-

shaped structures resembling those used in this study at larger sizes. In our model, it has been implicitly assumed that the shape morphology does not significantly affect the interaction of the QDs with the 2D surface fluxes of Ge adatoms. However, the real nanostructure shape can affect both BU delivery channels, directly from the plasma and via adatom surface migration. This is the case in the synthesis of carbon nanotip-like and related structures with variable shapes.[46]

We now turn our attention to discussing some of the salient features of plasma-aided nanoassembly. In one aspect, it has been discussed as a preferred route in enabling deterministic control in the growth and shape of nanostructures.[47] Another important feature is that high rates of material delivery from the plasma allow for faster QD growth compared to most of the conventional thermal deposition methods. The simulation results also indicate that uniform nanopatterns of size-uniform Ge/Si nanodots can be synthesized at surface temperatures as low as 600 K. This growth temperature is notably lower than those commonly used in thermal chemical vapor deposition (CVD). This can substantially expand the range of substrate materials that can host semiconductor QDs to include temperature-sensitive polymers, plastics, and ultrathin nanofilms. Another advantage is the possibility to use very short deposition processes (e.g., based on pulsed IPVD) not exceeding 1 s (see Table I); this is much shorter than the previously reported deposition times of CVD typically ranging anywhere between 0.5 and 40 min. We emphasize that plasma-based nanoassembly routes offer the possibility of controlling the dosing of specific (e.g., more complex) BUs.[16] For example, the Si(100) surface can be covered with a monolayer of atomic hydrogen in less than 0.5 s using an ion flux extracted from a 10 mTorr H_2 plasma at room temperature and an ionization degree of $\sim 10^{-4}$.[48] Plasma-based processes can also offer great precision in controlling the elemental composition of binary QDs, such as SiC/Si.[49] Another obvious advantage of the plasma-controlled self-organization approach is the ability of QDs to self-organize into ordered arrays without any lithographic prepattering or strain-driven site allocation. To summarize, by using plasma-based nanoassembly, it may eventually be possible to deliver controlled combinations of different plasma-generated species and arrange them selectively to fabricate intricate nanoassemblies.

In this article, we have explored the possibility of deterministic control of the quality of a nanodot pattern through specific manipulation of the surface temperature and the incoming flux of building units from the plasma. The QDs of our interest here are just an example of a low-dimensional nanostructure with outstanding prospects for optoelectronic and other applications. Beyond this, the scope of deterministic plasma-aided nanofabrication is set to launch into more complicated nanostructures and nanodevices.[50] The level of determinism may only be limited to the combination and sequence of the plasma and environmental adjustments. Finding suitable combinations to create the desired nanoassemblies in a plasma environment is the ultimate objective of plasma nanoscience.[50] The plasma route is a promising deterministic fabrication technique given the ability to ultimately transit toward commercial feasibility. The need for these new techniques and nanodevices is apparent as the current cost of lithographic manufacture increases and the operational limits of traditional semiconducting devices are inevitably approached.[51]

V. CONCLUSION

By means of multiscale hybrid numerical simulations, this paper has introduced an effective plasma-based technique to control self-organization within an array of Ge/Si QDs for establishing or improving spatial and dimensional order. It has been demonstrated that the self-organization phenomena can be explained by the ability of the system to maintain equal fluxes of adatoms about the perimeters of individual QDs. The dynamics of dot growth and displacement act accordingly to establish this self-organization scenario. Given the above results, several specific conclusions may assist in improving control and predictability of plasma-aided nanofabrication of Ge QD arrays on a Si(100) surface:

- Surface temperature is a factor that determines the mean size of QDs, with decreased temperatures producing larger dots while increased temperatures are shown to deteriorate the size uniformity over within the nanopattern.
- Plasma influx is a factor in the surface coverage of dots across the surface. Lower fluxes result in an increased final coverage (prior to coalescence) while for higher incoming fluxes the surface coverage is larger at the point of the maximum dot size uniformity. An apparent disadvantage of the lower influx is the extended growth time.
- The quality of the initial nanopatterns is an important factor in obtaining a high-level spatial order. However, some spatial and size variation is permitted as the growth process of our interest here does provide a substantial improvement in the spatial alignment and size uniformity.
- Spatial order may be further improved by decreasing the QD size in the initial nanopatterns.
- Spatial uniformity may be improved at temperatures as low as $\sim$600 K which is difficult to achieve via thermal deposition methods such as CVD.

Future work will aim at establishing ultimate control in the quality of the nanopatterns of Ge/Si and other QDs by determining the precise combination of the main process parameters and expanding the numerical simulations to account for the most essential features of QD internal structure and explore the effect of time-varying process parameters. Finally, our effort contributes to the improvement of present-day capabilities of plasma nanotools, with the ultimate goal to achieve fully deterministic, yet cost-efficient and microelectronic industry-compatible plasma-aided nanofabrication.

ACKNOWLEDGMENTS

We thank A. E. Rider for fruitful discussions and careful reading of the manuscript. This work was supported by the

Australian Research Council, the University of Sydney, and the International Research Network for Deterministic Plasma-Aided Nanofabrication.

[1]J. V. Barth, G. Costantini, and K. Kern, Nature **437**, 671 (2005).
[2]A. Karmous, A. Cuenat, A. Ronda, and I. Berbeziera, Appl. Phys. Lett. **85**, 26 (2004).
[3]R. M. Stevenson, R. J. Young, P. Atkinson, K. Cooper, D. A. Ritchie, and A. J. Shields, Nature **439**, 179 (2006).
[4]A. Imre, G. Csaba, L. Ji, A. Orlov, G. H. Bernstein, and W. Porod, Science **311**, 205 (2006).
[5]B. N. G. Giepmans, S. R. Adams, M. H. Ellisman, and R. Y. Tsien, Science **312**, 217 (2006).
[6]E. A. Stinaff, M. Scheibner, A. S. Bracker, I. V. Ponomarev, V. L. Korenev, M. E. Ware, M. F. Doty, T. L. Reinecke, and D. Gammon, Science **311**, 636 (2006).
[7]C. Lang, D. Nguyen-Manh, and D. J. H. Cockayne, J. Appl. Phys. **94**, 7067 (2003).
[8]A. I. Yakimov, A. V. Dvurechenskii, A. I. Nikiforov, and Y. Y. Proskuryakov, J. Appl. Phys. **89**, 5676 (2001).
[9]J. L. Gray, R. Hull, and J. A. Floro, J. Appl. Phys. **100**, 084312 (2006).
[10]P. A. Cain, H. Ahmed, and D. A. Williams, J. Appl. Phys. **92**, 346 (2002).
[11]T. M. Jovin, Nat. Biotechnol. **21**, 32 (2003).
[12]M. Brust, Nat. Mater. **4**, 364 (2005).
[13]A. Karmous, A. Cuenat, A. Ronda, and I. Berbeziera, Appl. Phys. Lett. **83**, 6401 (2004).
[14]S. Kohmoto, H. Nakamura, T. Ishikawa, S. Nishikawa, T. Nishimura, and K. Asakawa, Mater. Sci. Eng., B **88**, 292 (2002).
[15]J. Robertson, Mater. Today **10**, 36 (2007).
[16]K. Ostrikov, Rev. Mod. Phys. **77**, 489 (2005); S. V. Vladimirov and K. Ostrikov, Phys. Rep. **393**, 175 (2004).
[17]S. Sriraman, S. Agrawal, E. S. Aydil, and D. Maroudas, Nature **418**, 62 (2002).
[18]M. Keidar, Y. Raitses, A. Knapp, and A. M. Waas, Carbon **44**, 1022 (2006).
[19]M. Mozetic, U. Cvelbar, M. K. Sunkara, and S. Vaddiraju, Adv. Mater. **17**, 2138 (2002).
[20]Z. L. Tsakadze, K. Ostrikov, J. D. Long, and S. Xu, Diamond Relat. Mater. **13**, 1923 (2004); Z. L. Tsakadze, K. Ostrikov, and S. Xu, Surf. Coat. Technol. **191**, 49 (2005).
[21]M. Keidar and A. M. Waas, Nanotechnology **15**, 1571 (2004).
[22]S. Y. Huang, S. Y. Xu, J. D. Long, Z. Sun, and T. Chen, Phys. Plasmas **13**, 023506 (2006).
[23]M. Xu, S. Y. Xu, J. W. Chai, J. D. Long, and Y. C. Ee, Appl. Phys. Lett. **89**, 251904 (2006); K. Ostrikov, J. D. Long, P. P. Rutkevych, and S. Xu, Vacuum **80**, 1126 (2006).
[24]S. Xu, K. Ostrikov, J. D. Long, and S. Y. Huang, Vacuum **80**, 621 (2006); I. B. Denysenko, S. Xu, P. P. Rutkevych, J. D. Long, N. A. Azarenkov, and K. Ostrikov, J. Appl. Phys. **95**, 2713 (2004).
[25]V. Ligatchev, Rusli, and Z. Pan, Appl. Phys. Lett. **87**, 242903 (2005).
[26]V. Ligatchev, T. K. S. Wong, and S. F. Yoon, J. Appl. Phys. **95**, 7681 (2004).
[27]R. Nötzel, Z. Niu, M. Ramsteiner, H. P. Schoenherr, A. Tranpert, L. Daeweritz, and K. H. Ploog, Nature **392**, 56 (1998).
[28]H. Brune, M. Giovannini, K. Bromann, and K. Kern, Nature **394**, 451 (1998).
[29]E. Kasper and S. Heim, Appl. Surf. Sci. **224**, 3 (2004).
[30]A. Karmous, A. Cuenat, A. Ronda, I. Berbeziera, S. Atha, and R. Hull, Appl. Phys. Lett. **85**, 6401 (2004).
[31]A. Pascale, P. Gentile, J. Eymery, J. Meziere, A. Bavard, T. U. Schulli, and F. Fournel, Surf. Sci. **600**, 3187 (2006).
[32]M. De Seta, G. Capellini, and F. Evangelisti, Cryst. Res. Technol. **40**, 942 (2005).
[33]M. Keidar and I. D. Boyd, Appl. Phys. Lett. **87**, 121501 (2005); K. N. Ostrikov, M. Y. Yu, and H. Sugai, J. Appl. Phys. **86**, 2425 (1999).
[34]F. Rosei, J. Phys.: Condens. Matter **16**, S1373 (2004).
[35]C. Zhao, Y. H. Chen, C. X. Cui, B. Xu, L. K. Yu, W. Lei, J. Sun, and Z. G. Wang, Solid State Commun. **137**, 630 (2006).
[36]T. Takaki, T. Hasebe, and Y. Tomita, J. Cryst. Growth **287**, 495 (2006).
[37]I. Levchenko and O. Baranov, Vacuum **72**, 205 (2003).
[38]I. Levchenko and K. Ostrikov, Proc. SPIE **6039**, 60390L (2005).
[39]J. Shieh, T. S. Ko, H. L. Chen, B. T. Dai, and T. C. Chu, Chem. Vap. Deposition **10**, 265 (2004).
[40]V. Ligatchev and T. K. S. Wong, J. Electrochem. Soc. **152**, H58 (2005).
[41]E. A. Fitzgerald and D. G. Ast, "Method for reducing or eliminating interface defects in mismatched semiconductor epilayers," US Patent No. 5156995 (1992).
[42]A. D. Andreev, J. R. Downes, D. A. Faux, and E. P. O'Reilly, J. Appl. Phys. **86**, 297 (1999).
[43]G. Medeiros-Ribeiro, A. M. Bratkovski, T. I. Kamins, D. A. A. Ohlberg, and R. S. Williams, Science **279**, 353 (1998).
[44]D. J. Eaglesham and M. Cerullo, Phys. Rev. Lett. **64**, 1943 (1990).
[45]M. Tomitori, K. Watanabe, M. Kobayashi, and O. Nishikawa, Appl. Surf. Sci. **76–77**, 322 (1994).
[46]E. Tam, I. Levchenko, and K. Ostrikov, J. Appl. Phys. **100**, 036104 (2006); I. Levchenko, K. Ostrikov, M. Keidar, and S. Xu, Appl. Phys. Lett. **89**, 033109 (2006).
[47]I. Levchenko, K. Ostrikov, and E. Tam, Appl. Phys. Lett. **89**, 223108 (2006); I. Levchenko, K. Ostrikov, M. Keidar, and S. Xu, J. Appl. Phys. **98**, 064304 (2005).
[48]J. Shieh, C. H. Lin, and M. C. Yang, J. Phys. D **40**, 2242 (2007).
[49]A. E. Rider, I. Levchenko, and K. Ostrikov, J. Appl. Phys. **101**, 044306 (2007).
[50]K. Ostrikov, IEEE Trans. Plasma Sci. **35**, 127 (2007).
[51]K. Ostrikov and A. B. Murphy, J. Phys. D **40**, 2223 (2007).